
# Phonon-Assisted Photoluminescence from Indirect Excitons in Monolayers of Transition-Metal Dichalcogenides

NANO LETTERS

pubs.acs.org/NanoLett

Letter

# Phonon-Assisted Photoluminescence from Indirect Excitons in Monolayers of Transition-Metal Dichalcogenides

Samuel Brem,* August Ekman, Dominik Christiansen, Florian Katsch, Malte Selig, Cedric Robert, Xavier Marie, Bernhard Urbaszek, Andreas Knorr, and Ermin Malic

Cite This: *Nano Lett.* 2020, 20, 2849−2856

Read Online

ACCESS | Metrics & More | Article Recommendations | Supporting Information

**ABSTRACT:** The photoluminescence (PL) spectrum of transition-metal dichalcogenides (TMDs) shows a multitude of emission peaks below the bright exciton line, and not all of them have been explained yet. Here, we study the emission traces of phonon-assisted recombinations of indirect excitons. To this end, we develop a microscopic theory describing simultaneous exciton, phonon, and photon interaction and including consistent many-particle dephasing. We explain the drastically different PL below the bright exciton in tungsten- and molybdenum-based materials as the result of different configurations of bright and momentum-dark states. In good agreement with experiments, our calculations predict that $WSe_2$ exhibits clearly visible low-temperature PL signals stemming from the phonon-assisted recombination of momentum-dark K−K′ excitons.

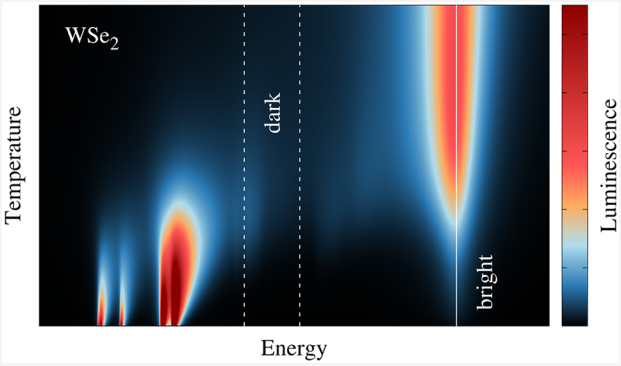


**KEYWORDS:** *dark excitons, photoluminescence, transition-metal dichalcogenides, exciton−phonon interaction, phonon side bands, microscopic model*



The cryogenic photoluminescence (PL) spectrum of two-dimensional (2D) semiconductors provides a powerful tool to study intriguing quantum phenomena invisible at room temperature or in linear optical experiments. The large variety of low-temperature emission features at energies below the bright exciton resonance indicates the existence of bound exciton configurations, such as trions, biexcitons,[1−6] and trapped excitons,[7,8] but could also result from the indirect recombination of momentum-dark exciton states.[9−16] The radiative decay of a momentum indirect electron−hole pair requires the simultaneous interaction with a phonon to fulfill the momentum conservation and is therefore very inefficient compared to the direct recombination of an exciton with zero center-of-mass momentum. However, in indirect semiconductors, where the momentum indirect exciton is located below the bright state, the low-temperature emission can exhibit strong phonon-assisted signals due to a large population of momentum-dark states, as depicted in Figure 1. Recently, the PL spectrum of hexagonal boron nitride has been shown to be dominated by phonon-assisted processes[17,18] resulting from an indirect band gap. Several theoretical and experimental studies have demonstrated that in tungsten-based monolayer materials, intervalley excitons are located below the optically bright exciton,[15,19−24] and recent experimental PL studies on hBN-encapsulated tungsten diselenide have revealed a multitude of low-temperature emission peaks whose microscopic origin still needs to be clarified.[3−5,9]

While the radiative decay of bright excitons has been extensively studied,[25−30] phonon-assisted exciton recombination has remained widely unexplored in the technologically promising field of TMD monolayers. In particular, a microscopic treatment of the large number of possible decay channels and the complex interplay between phonon-induced dephasing and recombination is challenging. In previous studies, restricted cases, such as optical phonon replicas of bright excitons, have been theoretically investigated within the polaron-frame[31,32] and nonmarkovian treatments of the density matrix.[33,34] However, there is so far no general theoretical framework for the phonon-assisted exciton recombination including optical and acoustic phonons as well as intra- and intervalley recombination channels on a microscopic footing.

Here, we present a fully microscopic model and low-temperature PL experiments demonstrating the emergence of pronounced phonon-assisted signals from momentum dark

**Received:** February 13, 2020
**Published:** February 21, 2020

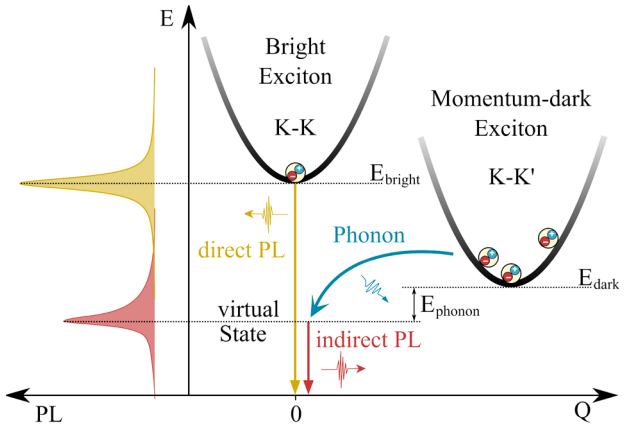


**Figure 1.** Sketch of direct and indirect decay channels for excitons showing the underlying scattering processes in the excitonic center-of-mass dispersion (right) and the corresponding PL signals (left). Momentum-dark excitons can decay by emitting or absorbing a phonon (blue arrow) and subsequently emitting a photon, which contributes to the indirect PL signal (red arrow).

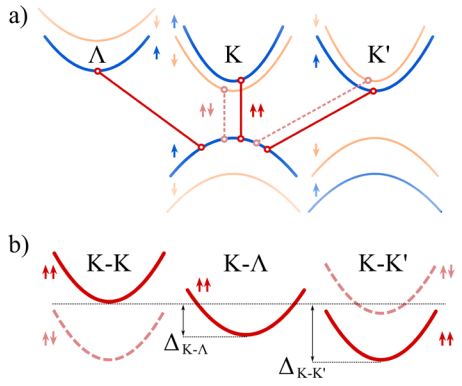


**Figure 2.** Schematic illustration of the (a) electronic and (b) corresponding excitonic dispersion around high-symmetry points in tungsten-based TMDs. While transitions involving electronic bands with the same spin are dipole allowed (red), the spin-dark excitons (pink dashed) require spin-flip processes. The specific spin-orbit coupling in tungsten-based TMDs renders the K−K′ as the lowest-lying spin-allowed exciton, in agreement with a recent ab initio calculation.[24]

excitons. Based on the fundamental equations-of-motion of the many-particle density matrix, we find an analytical formula which allows us to calculate temperature-dependent PL spectra. We apply the derived formula to calculate the luminescence spectrum of hBN-encapsulated TMD monolayers. For tungsten diselenide ($WSe_2$), our calculations predict clearly visible low-temperature emission features between 50 and 80 meV below the bright exciton, in good agreement with experimental observations. We identify these signals as phonon-assisted recombinations of momentum-dark K−K′ excitons. These peaks have been observed in several independent experiments, while their microscopic origin has not been clarified yet.[3,9,35] In contrast, for molybdenum diselenide ($MoSe_2$), we find no additional peaks and an opposite asymmetric broadening of the bright exciton resonance compared to $WSe_2$, which can be explained by the absence of lower lying momentum-dark excitons. Overall, our work provides new insights into phonon-assisted exciton luminescence and can be applied to determine emission spectra of arbitrary semiconducting materials, in particular including van der Waals stacked multilayers.

**Microscopic Model.** The central property determining the PL of a semiconductor is the electronic bandstructure in vicinity of the band gap. Therefore, we focus on the local band extrema, which in TMDs are located at the K, K′, and Λ point of the hexagonal Brillouin zone, cf. Figure 2a. Due to the strong Coulomb interaction in 2D materials, electrons and holes are tightly bound into excitons. Thereby, TMDs can host momentum direct intravalley excitons (K−K) as well as intervalley excitons, such as K−K′, where electrons and holes are located at the K′ and K point, respectively. The latter are optically dark, since the required momentum transfer cannot be provided by a photon. As a result of the peculiar ordering of spin-polarized electronic bands in tungsten-based TMDs,[36] the momentum-dark intervalley K−K′ excitons lies below the bright K−K excitons, cf. Figure 2b. When taking into account excitonic effects, the K−Λ excitons are also shifted below the bright K−K exciton due to the significantly larger mass of the Λ valley.

To set up a realistic model, we used ab initio input parameters for the electronic bandstructure, phonon dispersion, dielectric constants, and electron−phonon coupling elements.[36−38] The excitonic properties are derived in effective mass approximation by solving the Wannier equation.[39] In the following, we focus on the exemplary monolayers of tungsten diselenide ($WSe_2$). Moreover, we only consider spin-like exciton states, since their formation and recombination does not require spin-flip processes. The possible impact of spin-unlike K−K excitons is discussed later in the text. In Table 1, we have summarized all relevant exciton energies obtained from our Wannier model for different substrates as well as phonon energies in $WSe_2$ taken from ref 37. The phonon energies are in good agreement with experimental Raman measurements.[40,41] The calculated exciton binding energies and spectral exciton separations agree well with values found in literature using similar Wannier models,[42,43] ab initio studies,[24,44] and experiments.[45] In the following, we focus on hBN encapsulated samples, which have been shown to be less affected by undesirable external disorder effects.[46,47] The exact position of the K−Λ state relative to the bright exciton can be externally tuned via substrate-induced screening or strain.[23,24,48] In contrast, the valley-inverted spin-orbit coupling makes sure that the K−K′ exciton in tungsten-based TMDs is

**Table 1. Relevant Exciton Binding Energy $E_{bind}$, Spectral Exciton Separation $\Delta_{K-\Lambda}$, $\Delta_{K-K'}$ (with Respect to the Bright K−K State), and Phonon Energies in $WSe_2$[a]**

| exciton energies $WSe_2$ (meV) | | |
|---|---|---|
| | hBN enc. ($\varepsilon_r$ = 4.5) | vacuum ($\varepsilon_r$ = 1) |
| $E_{bind}(K-K\uparrow\uparrow)$ | 168 (172)[45] | 465 (450,[42] 480)[44] |
| $\Delta_{K-\Lambda}$ | −34 | −54 (−60)[24] |
| $\Delta_{K-K'}$ | −46 | −57 (−60)[24] |
| phonon energies $WSe_2$ (meV) | | |
| from ref [37] | Γ | Λ | K |
| TA/LA | 0 | 11.6/14.3 | 15.6/18 |
| TO/LO | 30.5/30.8 | 27.3/32.5 | 26.7/31.5 |
| A1 | 30.8 | 30.4 | 31 |

[a]Throughout this work, we consider hBN encapsulated samples. The free-standing results are given for direct comparison with literature values given in brackets. Phonon energies are taken from ref 37.


https://dx.doi.org/10.1021/acs.nanolett.0c00633
Nano Lett. 2020, 20, 2849−2856

always below the bright state independently of the used substrate.

After optical excitation and a quick thermalization process, excitons distribute across all valleys to form a Boltzman-like distribution in energy. Therefore, the energetically lowest momentum-dark states have, in particular at low temperatures, a much higher occupation then the bright exciton, so that in principle, PL signatures stemming from the indirect (phonon-assisted) recombination of dark excitons might become visible. In order to predict intensities and line shapes of the indirect PL signals, a sophisticated model of the mixed exciton−photon−phonon interactions is needed. Previous studies on PL phonon-side bands have used perturbative approaches or were restricted to specific phonon modes and intravalley processes. Here, we develop a more universal approach including acoustic and optical modes, intra- and intervalley scattering, all temperature ranges, and a self-consistent description of phonon-induced broadening and recombination.

We derive the PL signal from the many-particle density matrix of an interacting system of electrons, phonons and photons. Throughout this work, we assume an excitation density far away from the exciton-Mott transition and model excitons as a gas of non-interacting bosons. In this regime, the many-particle physics of an undoped monolayer can be described by the excitonic Hamiltonian,[33,49−51] which in the rotating frame[52] reads

$$H = \sum_{\mu \mathbf{Q}_\parallel} E^{\mu}_{\mathbf{Q}_\parallel} a^{\dagger}_{\mu \mathbf{Q}_\parallel} a_{\mu \mathbf{Q}_\parallel} + \sum_{\alpha \mathbf{q}_\parallel} \Omega^{\alpha}_{\mathbf{q}_\parallel} b^{\dagger}_{\alpha \mathbf{q}_\parallel} b_{\alpha \mathbf{q}_\parallel} + \sum_{\sigma \mathbf{k}} \omega^{\sigma}_{\mathbf{k}} c^{\dagger}_{\sigma \mathbf{k}} c_{\sigma \mathbf{k}} + \sum_{\mu \sigma \mathbf{k}} (M^{\mu}_{\sigma \mathbf{k}} c^{\dagger}_{\sigma \mathbf{k}} a_{\mu \mathbf{k}_\parallel} + M^{\mu *}_{\sigma \mathbf{k}} a^{\dagger}_{\mu \mathbf{k}_\parallel} c_{\sigma \mathbf{k}}) + \sum_{\nu \mu \mathbf{Q}_\parallel \alpha \mathbf{q}_\parallel} D^{\nu \mu}_{\alpha \mathbf{q}_\parallel} a^{\dagger}_{\nu \mathbf{Q}_\parallel + \mathbf{q}_\parallel} a_{\mu \mathbf{q}_\parallel} (b_{\alpha \mathbf{q}_\parallel} + b^{\dagger}_{\alpha, -\mathbf{q}_\parallel}) \tag{1}$$

where $\mathbf{k}_\parallel$ denotes the component of the momentum $\mathbf{k}$ parallel to the monolayer plane. We use annihilation (creation) operators $a^{(\dagger)}_{\mu \mathbf{Q}_\parallel}$, $b^{(\dagger)}_{\alpha \mathbf{q}_\parallel}$ and $c^{(\dagger)}_{\sigma \mathbf{k}}$ for excitons in the state $\mu$, phonons in the mode $\alpha$, and photons with the polarization $\sigma$, respectively. Moreover, the corresponding dispersions for the three particle species are given by $E^{\mu}_{\mathbf{Q}_\parallel}$, $\Omega^{\alpha}_{\mathbf{q}_\parallel}$ and $\omega^{\sigma}_{\mathbf{k}}$. Here, the excitonic bandstructure $E^{\mu}_{\mathbf{Q}_\parallel}$ is decomposed into valleys around energetic extrema, cf. Figure 2, where excitons can be described as free particles with effective valley masses. The exciton index $\mu$ acts as a compound index containing main, angular, spin, and valley quantum numbers. The second line of eq 1 describes the conversion of excitons to photons and vice versa under conservation of the in-plane momentum, whose probability is determined by the exciton-photon matrix element $M^{\mu}_{\sigma \mathbf{k}}$. Finally, excitons can scatter from the state ($\mu$, $\mathbf{Q}_\parallel$) to ($\nu$, $\mathbf{Q}_\parallel + \mathbf{q}_\parallel$) by emitting or absorbing a phonon, guided by the exciton−phonon matrix element $D^{\nu \mu}_{\alpha \mathbf{q}_\parallel}$. Details about the calculation of these matrix elements are given in previous works[15,53,54] and can also be found in the Supporting Information.

In this framework, the PL can be determined from the temporal change of the photon density $n_{\mathbf{k}} = \langle c^{\dagger}_{\mathbf{k}} c_{\mathbf{k}} \rangle$.[55] Applying the Heisenberg equation of motion, we find coupled differential equations for the photon density, the polarization $\mathcal{S}^{\mu}_{\mathbf{k}} = \langle c^{\dagger}_{\mathbf{k}} a_{\mu \mathbf{k}_\parallel} \rangle$, the phonon-assisted polarization $\mathcal{U}^{\mu,\pm}_{\mathbf{kq}} = \langle c^{\dagger}_{\mathbf{k}} b^{(\dagger)}_{\mp \mathbf{q}} a_{\mu \mathbf{k}_\parallel - \mathbf{q}} \rangle$ and further higher-order correlations. We factorize appearing many-particle expectation values according to the cluster expansion scheme.[56] Here, we disregard contributions connected to multiphonon emission/absorption. However, we include correlations giving rise to the phonon-induced dephasing $\Gamma^{\mu}_{\mathbf{Q}} = \pi \sum_{\nu \mathbf{q}, \pm} |D^{\mu \nu}_{\mathbf{q}}|^2 \eta^{\pm}_{\mathbf{q}} \delta(E^{\mu}_{\mathbf{Q}} \pm \Omega_{\mathbf{q}} - E^{\nu}_{\mathbf{Q}+\mathbf{q}})$ as well as the radiative dephasing for exciton states within the light cone $\gamma^{\mu}_{\mathbf{k}_\parallel} = \pi \sum_{\mathbf{k}'} |M^{\mu}_{\mathbf{k}}|^2 \delta_{\mathbf{k}'_\parallel \mathbf{k}_\parallel} \delta(E^{\mu}_{\mathbf{k}_\parallel} - \omega_{\mathbf{k}'})$. A detailed study on these dephasing rates can be found in our previous studies.[15,47] It is of key importance to include these dephasing contributions in the truncation scheme. In particular, we find that phonon-assisted recombinations via virtual states close to the actual bright state are physically equivalent to a phonon-induced broadening of the bright state. Therefore, a phenomenological inclusion of dephasing rates can give rise to nonphysical negative luminescence signals. A detailed derivation and discussion is provided in the Supporting Information. Finally, we find the following analytic expression for the $\sigma$-polarized photon flux emitted in perpendicular direction with respect to the monolayer:

$$I_{\sigma}(E) = \frac{2}{\hbar} \sum_{\mu} \frac{|M^{\mu}_{\sigma}|^2}{(E^{\mu}_0 - E)^2 + (\gamma^{\mu}_{\sigma 0} + \Gamma^{\mu}_0)^2} \times \left( \gamma^{\mu}_{\sigma 0} N^{\mu}_0 + \sum_{\nu \mathbf{q}, \alpha \pm} |D^{\mu \nu}_{\alpha \mathbf{q}}|^2 N^{\nu}_{\mathbf{q}} \eta^{\pm}_{\alpha \mathbf{q}} \frac{\Gamma^{\nu}_{\mathbf{q}}}{(E^{\nu}_{\mathbf{q}} \pm \Omega^{\alpha}_{\mathbf{q}} - E)^2 + (\Gamma^{\nu}_{\mathbf{q}})^2} \right) \tag{2}$$

where $\eta^{\pm}_{\mathbf{q}} = 1/2 \mp 1/2 + \langle b^{\dagger}_{\mathbf{q}} b_{\mathbf{q}} \rangle$ denotes the relevant phonon occupation factor for absorption/emission, and $N^{\mu}_{\mathbf{Q}} = \langle a^{\dagger}_{\mu \mathbf{Q}} a_{\mu \mathbf{Q}} \rangle$ represents the exciton occupation. The first term reflects the Lorentz-shaped response of the direct recombination of bright excitons, with a small difference that the phonon dephasing only appears in the denominator. However, for energies $E \approx E_0$, the second term containing the scattering contributions is proportional to the phonon-assisted in-scattering to the bright state, so that close to thermal equilibrium, the second term in the brackets becomes $\Gamma^{\mu}_0 N^{\mu}_0$. Therefore, in the resonant case, eq 2 can be well approximated with the exciton Elliot formula:[39]

$$I_{\sigma}(E)_{E \approx E_0} = \frac{2}{\hbar} \sum_{\mu} \frac{|M^{\mu}_{\sigma}|^2 (\gamma^{\mu}_{\sigma 0} + \Gamma^{\mu}_0)}{(E^{\mu}_0 - E)^2 + (\gamma^{\mu}_{\sigma 0} + \Gamma^{\mu}_0)^2} N^{\mu}_0 \tag{3}$$

The second part of eq 2 containing phonon-assisted decay channels agrees with luminescence formulas derived in previous studies[31,32] for optical phonon replicas in the polaron picture. The advantage of our approach is that it consistently includes broadening and additional decay channels allowing to quantitatively compare line shapes and intensities of bright and dark states. The equation can be generally applied to other semiconducting systems as long as the band edge excitations are of excitonic nature. We have used general compound indices for the excitons allowing to include phonon-assisted transitions involving other exciton states as the ones studied in this work, such as phonon-mediated spin-flip transitions and layer-hybridized Moire excitons as well as localized/charge trapped excitons.

Note that the model does not account for exciton−exciton interaction or the presence of residual free charge carriers,


https://dx.doi.org/10.1021/acs.nanolett.0c00633
Nano Lett. 2020, 20, 2849−2856

which can enable further bound many-particle states, such as biexcitons or trions. The latter gives rise to well studied low-temperature PL features[1−5,57] below the bright exciton.

**Results.** Now we apply the derived eq 2 together with the calculated exciton energies and wave functions to calculate the PL signal of the multivalley exciton landscape. Figure 3 shows calculated PL spectra for hBN-encapsulated monolayer $WSe_2$ at four different temperatures. In addition to the full spectra calculated from eq 2 (color shaded), we also present the spectra in the case of $\Gamma_q^\nu \to 0$ (solid line). This corresponds to $\delta$ functions in the brackets of eq 2, requiring strict energy conservation for the conversion from an exciton to a phonon and photon. The sharp steps in the solid line conveniently illustrate the multitude of exciton valleys and phonon modes contributing to the overall PL signal. Here, each step in the spectrum corresponds to a transition from the energetic minimum of a certain valley, while absorbing/emitting a phonon.

At 300 and 150 K, the PL spectrum is dominated by the bright exciton resonance, but already here, phonon-assisted indirect recombinations have a significant impact resulting in an asymmetric resonance. At energies larger than $E_0$, the signal is mainly shaped by recombinations of small momentum excitons in the K−K valley, which scatter to virtual states in the light cone via low-energy acoustic phonons. For energies smaller than $E_0$, a much larger broadening is observed. This can be ascribed to K−K excitons emitting optical phonons and, more importantly, to the indirect decay of momentum-dark intervalley excitons. Our Wannier model predicts that the K−Λ and K−K′ excitons are located about 34 and 46 meV below the bright exciton, respectively. These momentum-dark states can perform indirect PL transitions as depicted in Figure 1, preferably to virtual states close to the bright exciton, yielding the asymmetric peak shape at room temperature.

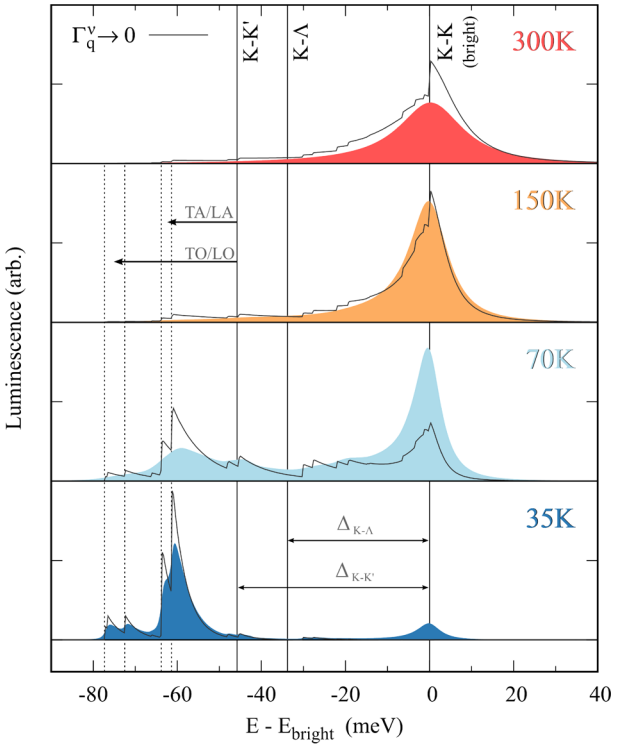


**Figure 3.** PL spectra of hBN-encapsulated $WSe_2$ monolayers at four different temperatures. Together with the full simulation (colored curves), we also show the solution for zero dark-state dephasing (thin solid lines). At higher temperatures, the lower-lying momentum-dark states K−K′ and K−Λ give rise to a strong asymmetric broadening of the bright exciton resonance toward lower energies. For low temperatures, the PL signal exhibits indirect peaks stemming from the phonon-assisted recombination of momentum-dark excitons.

At low temperatures, the optical response shifts toward multiple indirect PL peaks below the bright exciton stemming from the phonon-assisted recombination of the energetically lowest K−K′ exciton. The observed temperature dependence is a result of a competition between oscillator strength and occupation probability. The phonon-assisted peaks become only visible at low temperatures because here the exciton distribution becomes very narrow in energy. Therefore, excitons are "forced" to take the unlikely indirect recombination pathway via a virtual state, since it is even more unlikely to occupy the energetically higher bright state. This temperature behavior is analogue to localized excitons, which only become visible for thermal energies smaller than the trapping energy.

The predicted low-temperature PL signals at about −60 meV (K−K′, acoustic K phonon-assisted) and −75 meV (K−K′, optical K phonon-assisted) correspond well to experimentally observed but so far not fully explained PL peaks in hBN-encapsulated samples tuned to charge neutrality. In agreement with our theory, these peaks are not visible in reflection/absorption spectra.[58] We have also performed calculations for tungsten disulfide ($WS_2$) monolayers and find the same qualitative temperature trend. Here, the phonon-assisted peaks are located at about −70 and −90 meV (cf. Supporting Information), resulting from slightly different exciton and phonon dispersions.

In Figure 4 we directly compare an experimentally measured PL spectrum with our simulation. The blue shaded curve shows the PL measured at $T$ = 15 K for hBN-encapsulated $WSe_2$ at charge neutrality. Details about the experiment can be found in ref 3. The red line shows the corresponding calculated spectrum. For a better comparison, the calculated spectrum in Figure 4 was convoluted with a 1 meV broad Gaussian to simulate disorder in the experiment, viz. small statistical fluctuations of resonance energies resulting from inhomogeneities throughout the sample. Figure 4 illustrates that the

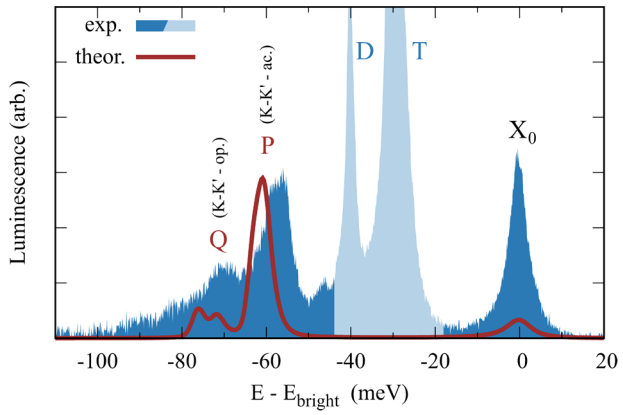


**Figure 4.** Direct comparison between experiment and theory. The blue shaded curve shows the PL spectrum measured on hBN-encapsulated $WSe_2$ at charge neutrality at $T$ = 15 K. The red line shows the corresponding simulated spectrum. Peaks P and Q denote the acoustic and optical phonon-assisted recombination of K−K′ excitons.


https://dx.doi.org/10.1021/acs.nanolett.0c00633
Nano Lett. 2020, 20, 2849−2856

theoretically predicted PL features from the momentum-dark K−K′ exciton agree well with the experimentally observed resonances between 50 and 80 meV below the bright exciton denoted with P and Q. The two pronounced peaks around 40 and 30 meV below the bright state (denoted with D and T) have been assigned to spin-dark states[4] and charge defect bound trions,[59] respectively. They are beyond the scope of this work.

When comparing peak intensities in theory and experiment we find quantitative differences in the height of the bright exciton $X_0$ and the phonon side peaks P and Q. This deviation could result from numerical inaccuracies in the exciton−phonon matrix element, for example, resulting from the applied deformation potential approximation.[37] Moreover, the presence of the neglected defect-bound trions (T) and the spin-forbidden exciton (D) could influence the oscillator strength and occupation of the bright state. In general, the complex interplay of optical pumping and phonon-induced relaxations as well as radiative and nonradiative recombination, which at low temperatures take place on comparable time scales, could result in quasi-equilibrium distributions in the experiment that deviate from the assumed Boltzmann distribution. However, we find a good qualitative agreement for the temperature dependence of peak shapes and intensity ratios. In the Supporting Information, we show further spectra measured on the same system at different temperatures. We find that the intensity of P and Q relative to $X_0$ increases, while the slope on the high-energy side of the peak P becomes steeper with decreasing temperature. Both findings are consistent with our model, since both the intensity as well as the peak shape of the phonon-assisted emission are determined by the energetic distribution of excitons $\propto \exp(-E/k_BT)$.

Moreover, we have summarized several independent PL measurements on hBN-encapsulated $WSe_2$[3−5] in the Supporting Information. All of these studies show the phonon-assisted peaks discussed above. Interestingly, the strongest peak denoted as P in Figure 4 (attributed in our work to the acoustic phonon-assisted decay of K−K′ excitons) shows a double peak structure in experiments performed at 4 K. The lower one of the two peaks (P2) splits in magnetic fields into two resonances with the same *g*-factor as the spin-dark D peak.[60] In contrast, the other peak (P1) shows a different behavior in magnetic fields, cf. Supporting Information. The studies in refs 60 and 61 suggest that P2 is most likely a phonon replica of the spin-dark exciton D, involving chiral E″ phonons for the necessary spin-flip. However, the origin of the second peak P1 has not been explained yet. Polarization resolved measurements show both peaks P1 and P2 in copolarized measurements, while the energetically higher P1 is much weaker in cross-polarized set-ups.[4] Both, the magnetic field dependence from ref 60 as well as the polarization dependent measurements in ref 4 support our assignment of P1 to the phonon-assisted recombination of K−K′ spin-like excitons, cf. Supporting Information for further details.

Finally, we compare our results obtained for $WSe_2$ with molybdenum-based TMDs, cf. Figure 5. Here, we show a continuous temperature study of the PL spectrum for (a) $WSe_2$ and (b) $MoSe_2$. In tungsten-based TMDs, the lower-lying K−Λ and K−K′ valley provide a continuous density of (momentum-dark) states below the bright exciton, yielding an asymmetric broadening of the bright exciton peak toward lower energies. In contrast, for $MoSe_2$, the bright state constitutes the global minimum of the exciton dispersion

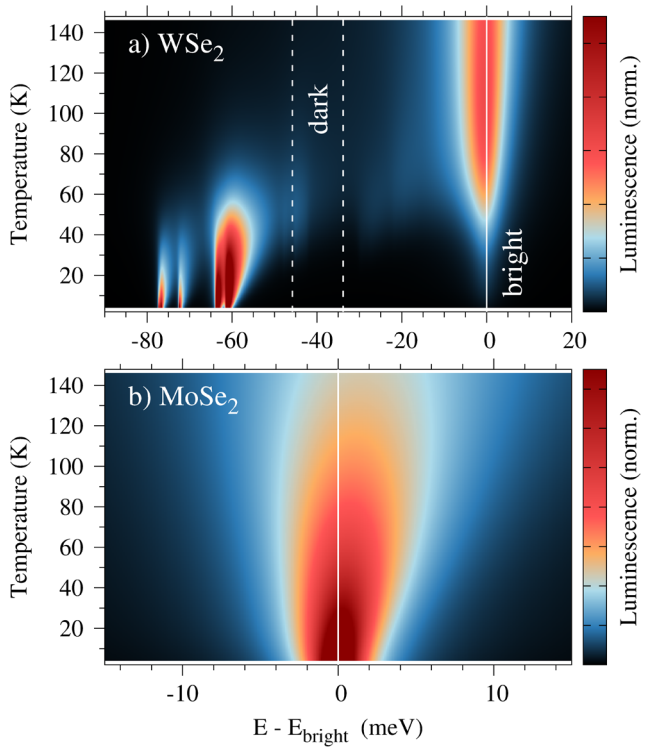


**Figure 5.** Temperature-dependent PL spectra calculated for (a) $WSe_2$ and (b) $MoSe_2$. For each temperature, the spectra have been normalized to the integrated PL. While $WSe_2$ shows a clearly asymmetric broadening toward lower energies and distinct indirect peaks at low temperatures, $MoSe_2$ has no additional indirect peaks and is more strongly broadened toward higher energies.

calculated in our Wannier model. Therefore, there are no phonon-assisted PL peaks below the bright state, and the main peak is asymmetrically broadened toward higher energies, cf. Figure 5b. Here the broadening of the low energy side of the main line is predominantly given by the energy uncertainty of the bright state giving rise to a Lorentzian shape. In contrast, the high-energy side is additionally shaped by the decay of small momentum excitons in the K−K valley assisted by long-range acoustic phonons, which agrees with the findings in ref 34.

In summary, we have presented an analytical expression for the phonon-assisted exciton PL from momentum-dark excitons which allows to model the emission spectrum of an arbitrary semiconducting material. When applying our model to the luminescence of $WSe_2$, we find a good agreement with experiment clear PL signals stemming from momentum-dark intervalley excitons, potentially explaining the origin of so far observed but unidentified PL peaks. In contrast, $MoSe_2$ does not exhibit indirect PL peaks and shows an opposite asymmetric broadening which is consistent with the absence of lower-lying momentum-dark exciton states. Our work will trigger future experimental and theoretical studies on momentum-dark exciton PL and in particular addressing exciton thermalization and diffusion.

## ■ ASSOCIATED CONTENT

### Supporting Information

The Supporting Information is available free of charge at https://pubs.acs.org/doi/10.1021/acs.nanolett.0c00633.



https://dx.doi.org/10.1021/acs.nanolett.0c00633
Nano Lett. 2020, 20, 2849−2856

Derivation of the equations of motion, many-particle dephasing and PL formula; details on the calculation of excitonic energies, wave functions and matrix elements; summary of supporting PL spectra published in other works; time dependent PL of P1 and P2; temperature dependent PL spectra of $WSe_2$; calculated energies and PL in $WS_2$ (PDF)

## AUTHOR INFORMATION


### Corresponding Author

**Samuel Brem** − *Department of Physics, Chalmers University of Technology, 41296 Gothenburg, Sweden;* orcid.org/0000-0001-8823-1302; Email: brem@chalmers.se

### Authors

**August Ekman** − *Department of Physics, Chalmers University of Technology, 41296 Gothenburg, Sweden*

**Dominik Christiansen** − *Institute of Theoretical Physics, Technical University Berlin, 10623 Berlin, Germany*

**Florian Katsch** − *Institute of Theoretical Physics, Technical University Berlin, 10623 Berlin, Germany*

**Malte Selig** − *Institute of Theoretical Physics, Technical University Berlin, 10623 Berlin, Germany;* orcid.org/0000-0003-0022-412X

**Cedric Robert** − *Laboratoire de Physique et Chimie des Nano-objets (LPCNO), Université de Toulouse, INSA-CNRS-UPS, 31077 Toulouse, France*

**Xavier Marie** − *Laboratoire de Physique et Chimie des Nano-objets (LPCNO), Université de Toulouse, INSA-CNRS-UPS, 31077 Toulouse, France*

**Bernhard Urbaszek** − *Laboratoire de Physique et Chimie des Nano-objets (LPCNO), Université de Toulouse, INSA-CNRS-UPS, 31077 Toulouse, France*

**Andreas Knorr** − *Institute of Theoretical Physics, Technical University Berlin, 10623 Berlin, Germany*

**Ermin Malic** − *Department of Physics, Chalmers University of Technology, 41296 Gothenburg, Sweden*

Complete contact information is available at: https://pubs.acs.org/10.1021/acs.nanolett.0c00633


### Notes

The authors declare no competing financial interest.

## ACKNOWLEDGMENTS

The Chalmers group acknowledges financial support from the European Unions Horizon 2020 research and innovation program under grant agreement no. 785219 (Graphene Flagship) as well as from the Swedish Research Council (VR, project no. 2018-00734). The TUB group was funded by the Deutsche Forschungsgemeinschaft (DFG) via projects number 182087777 in SFB 951 (project B12, D.C., M.S., and A.K.) and KN 427/11-1 (F.K. and A.K.) as well as and by the European Unions Horizon 2020 research and innovation program under grant agreements no. 734690 (SONAR, A.K.). F.K. thanks the Berlin School of Optical Sciences and Quantum Technology. C.R. and B.U. acknowledge funding from ANR 2D-vdW-Spin, ANR VallEx, Labex NEXT projects VWspin and MILO, ITN Spin-NANO Marie Sklodowska-Curie grant agreement no. 676108 and ITN 4PHOTON no. 721394.

## REFERENCES


(1) Mak, K. F.; He, K.; Lee, C.; Lee, G. H.; Hone, J.; Heinz, T. F.; Shan, J. Tightly bound trions in monolayer MoS2. *Nat. Mater.* **2013**, *12*, 207.

(2) Wang, G.; Bouet, L.; Lagarde, D.; Vidal, M.; Balocchi, A.; Amand, T.; Marie, X.; Urbaszek, B. Valley dynamics probed through charged and neutral exciton emission in monolayer WSe2. *Phys. Rev. B: Condens. Matter Mater. Phys.* **2014**, *90*, 075413.

(3) Courtade, E.; Semina, M.; Manca, M.; Glazov, M.; Robert, C.; Cadiz, F.; Wang, G.; Taniguchi, T.; Watanabe, K.; Pierre, M.; et al. Charged excitons in monolayer WSe2: experiment and theory. *Phys. Rev. B: Condens. Matter Mater. Phys.* **2017**, *96*, 085302.

(4) Ye, Z.; Waldecker, L.; Ma, E. Y.; Rhodes, D.; Antony, A.; Kim, B.; Zhang, X.-X.; Deng, M.; Jiang, Y.; Lu, Z.; et al. Efficient generation of neutral and charged biexcitons in encapsulated WSe2 monolayers. *Nat. Commun.* **2018**, *9*, 3718.

(5) Barbone, M.; Montblanch, A. R.-P.; Kara, D. M.; Palacios-Berraquero, C.; Cadore, A. R.; De Fazio, D.; Pingault, B.; Mostaani, E.; Li, H.; Chen, B.; et al. Charge-tuneable biexciton complexes in monolayer WSe2. *Nat. Commun.* **2018**, *9*, 3721.

(6) He, M.; Rivera, P.; Van Tuan, D.; Wilson, N. P.; Yang, M.; Taniguchi, T.; Watanabe, K.; Yan, J.; Mandrus, D. G.; Yu, H.; Dery, H.; Yao, W.; Xu, X. *Nat. Commun.* **2020**, *11*, 618.

(7) Tonndorf, P.; Schmidt, R.; Schneider, R.; Kern, J.; Buscema, M.; Steele, G. A.; Castellanos-Gomez, A.; van der Zant, H. S.; de Vasconcellos, S. M.; Bratschitsch, R. Single-photon emission from localized excitons in an atomically thin semiconductor. *Optica* **2015**, *2*, 347−352.

(8) Zhang, S.; Wang, C.-G.; Li, M.-Y.; Huang, D.; Li, L.-J.; Ji, W.; Wu, S. Defect Structure of Localized Excitons in a WSe2Monolayer. *Phys. Rev. Lett.* **2017**, *119*, 046101.

(9) Lindlau, J.; Robert, C.; Funk, V.; Förste, J.; Förg, M.; Colombier, L.; Neumann, A.; Courtade, E.; Shree, S.; Taniguchi, T., et al. Identifying optical signatures of momentum-dark excitons in transition metal dichalcogenide monolayers. *arXiv (Mesoscale and Nanoscale Physics)*, October 25, 2017, 1710.00988, ver. 2. https://arxiv.org/abs/1710.00988 (accessed Oct 25, 2017)

(10) Lindlau, J.; Selig, M.; Neumann, A.; Colombier, L.; Förste, J.; Funk, V.; Förg, M.; Kim, J.; Berghäuser, G.; Taniguchi, T.; et al. The role of momentum-dark excitons in the elementary optical response of bilayer WSe2. *Nat. Commun.* **2018**, *9*, 2586.

(11) Koperski, M.; Molas, M. R.; Arora, A.; Nogajewski, K.; Slobodeniuk, A. O.; Faugeras, C.; Potemski, M. Optical properties of atomically thin transition metal dichalcogenides: observations and puzzles. *Nanophotonics* **2017**, *6*, 1289−1308.

(12) Song, Y.; Dery, H. Transport theory of monolayer transition-metal dichalcogenides through symmetry. *Phys. Rev. Lett.* **2013**, *111*, 026601.

(13) Mueller, T.; Malic, E. Exciton physics and device application of two-dimensional transition metal dichalcogenide semiconductors. *npj 2D Mater. Appl.* **2018**, *2*, 29.

(14) Malic, E.; Selig, M.; Feierabend, M.; Brem, S.; Christiansen, D.; Wendler, F.; Knorr, A.; Berghäuser, G. Dark excitons in transition metal dichalcogenides. *Physical Review Materials* **2018**, *2*, 014002.

(15) Selig, M.; Berghäuser, G.; Raja, A.; Nagler, P.; Schüller, C.; Heinz, T. F.; Korn, T.; Chernikov, A.; Malic, E.; Knorr, A. Excitonic linewidth and coherence lifetime in monolayer transition metal dichalcogenides. *Nat. Commun.* **2016**, *7*, 13279.

(16) Feierabend, M.; Berghäuser, G.; Knorr, A.; Malic, E. Proposal for dark exciton based chemical sensors. *Nat. Commun.* **2017**, *8*, 14776.

(17) Cassabois, G.; Valvin, P.; Gil, B. Hexagonal boron nitride is an indirect bandgap semiconductor. *Nat. Photonics* **2016**, *10*, 262.

(18) Paleari, F.; Miranda, H. P.; Molina-Sánchez, A.; Wirtz, L. Exciton-Phonon Coupling in the Ultraviolet Absorption and Emission Spectra of Bulk Hexagonal Boron Nitride. *Phys. Rev. Lett.* **2019**, *122*, 187401.

(19) Zhang, X.-X.; You, Y.; Zhao, S. Y. F.; Heinz, T. F. Experimental evidence for dark excitons in monolayer WSe2. *Phys. Rev. Lett.* **2015**, *115*, 257403.
(20) Dery, H.; Song, Y. Polarization analysis of excitons in monolayer and bilayer transition-metal dichalcogenides. *Phys. Rev. B: Condens. Matter Mater. Phys.* **2015**, *92*, 125431.
(21) Echeverry, J.; Urbaszek, B.; Amand, T.; Marie, X.; Gerber, I. Splitting between bright and dark excitons in transition metal dichalcogenide monolayers. *Phys. Rev. B: Condens. Matter Mater. Phys.* **2016**, *93*, 121107.
(22) Berghäuser, G.; Steinleitner, P.; Merkl, P.; Huber, R.; Knorr, A.; Malic, E. Mapping of the dark exciton landscape in transition metal dichalcogenides. *Phys. Rev. B: Condens. Matter Mater. Phys.* **2018**, *98*, No. 020301.
(23) Niehues, I.; Schmidt, R.; Drüppel, M.; Marauhn, P.; Christiansen, D.; Selig, M.; Berghäuser, G.; Wigger, D.; Schneider, R.; Braasch, L.; et al. Strain control of exciton−phonon coupling in atomically thin semiconductors. *Nano Lett.* **2018**, *18*, 1751−1757.
(24) Deilmann, T.; Thygesen, K. S. Finite-momentum exciton landscape in mono-and bilayer transition metal dichalcogenides. *2D Mater.* **2019**, *6*, 035003.
(25) Moody, G.; Kavir Dass, C.; Hao, K.; Chen, C.-H.; Li, L.-J.; Singh, A.; Tran, K.; Clark, G.; Xu, X.; Berghauser, G.; Malic, E.; Knorr, A.; Li, X.; et al. Intrinsic homogeneous linewidth and broadening mechanisms of excitons in monolayer transition metal dichalcogenides. *Nat. Commun.* **2015**, *6*, 8315.
(26) Palummo, M.; Bernardi, M.; Grossman, J. C. Exciton radiative lifetimes in two-dimensional transition metal dichalcogenides. *Nano Lett.* **2015**, *15*, 2794−2800.
(27) Steinhoff, A.; Kim, J.-H.; Jahnke, F.; Rösner, M.; Kim, D.-S.; Lee, C.; Han, G. H.; Jeong, M. S.; Wehling, T.; Gies, C. Efficient excitonic photoluminescence in direct and indirect band gap monolayer MoS2. *Nano Lett.* **2015**, *15*, 6841−6847.
(28) Pöllmann, C.; Steinleitner, P.; Leierseder, U.; Nagler, P.; Plechinger, G.; Porer, M.; Bratschitsch, R.; Schüller, C.; Korn, T.; Huber, R. Resonant internal quantum transitions and femtosecond radiative decay of excitons in monolayer WSe 2. *Nat. Mater.* **2015**, *14*, 889.
(29) Robert, C.; Lagarde, D.; Cadiz, F.; Wang, G.; Lassagne, B.; Amand, T.; Balocchi, A.; Renucci, P.; Tongay, S.; Urbaszek, B.; et al. Exciton radiative lifetime in transition metal dichalcogenide monolayers. *Phys. Rev. B: Condens. Matter Mater. Phys.* **2016**, *93*, 205423.
(30) Wang, H.; Zhang, C.; Chan, W.; Manolatou, C.; Tiwari, S.; Rana, F. Radiative lifetimes of excitons and trions in monolayers of the metal dichalcogenide MoS2. *Phys. Rev. B: Condens. Matter Mater. Phys.* **2016**, *93*, 045407.
(31) Feldtmann, T.; Kira, M.; Koch, S. W. Phonon sidebands in semiconductor luminescence. *Phys. Status Solidi B* **2009**, *246*, 332−336.
(32) Feldtmann, T.; Kira, M.; Koch, S. W. Theoretical analysis of higher-order phonon sidebands in semiconductor luminescence spectra. *J. Lumin.* **2010**, *130*, 107−113.
(33) Chernikov, A.; Bornwasser, V.; Koch, M.; Chatterjee, S.; Böttge, C.; Feldtmann, T.; Kira, M.; Koch, S. W.; Wassner, T.; Lautenschläger, S.; et al. Phonon-assisted luminescence of polar semiconductors: Fröhlich coupling versus deformation-potential scattering. *Phys. Rev. B: Condens. Matter Mater. Phys.* **2012**, *85*, 035201.
(34) Shree, S.; Semina, M.; Robert, C.; Han, B.; Amand, T.; Balocchi, A.; Manca, M.; Courtade, E.; Marie, X.; Taniguchi, T.; et al. Observation of exciton-phonon coupling in MoSe2 monolayers. *Phys. Rev. B: Condens. Matter Mater. Phys.* **2018**, *98*, 035302.
(35) Ye, Z.; Waldecker, L.; Ma, E. Y.; Rhodes, D.; Antony, A.; Kim, B.; Zhang, X.-X.; Deng, M.; Jiang, Y.; Lu, Z.; Smirnov, D.; Watanabe, K.; Taniguchi, T.; Hone, J.; Heinz, T. F. Efficient generation of neutral and charged biexcitons in encapsulated WSe2 monolayers. *Nat. Commun.* **2018**, *9*, 3718.
(36) Kormányos, A.; Burkard, G.; Gmitra, M.; Fabian, J.; Zólyomi, V.; Drummond, N. D.; Falko, V. k· p theory for two-dimensional transition metal dichalcogenide semiconductors. *2D Mater.* **2015**, *2*, 022001.
(37) Jin, Z.; Li, X.; Mullen, J. T.; Kim, K. W. Intrinsic transport properties of electrons and holes in monolayer transition-metal dichalcogenides. *Phys. Rev. B: Condens. Matter Mater. Phys.* **2014**, *90*, 045422.
(38) Laturia, A.; Van de Put, M. L.; Vandenberghe, W. G. Dielectric properties of hexagonal boron nitride and transition metal dichalcogenides: from monolayer to bulk. *npj 2D Mater. Appl.* **2018**, *2*, 6.
(39) Koch, S.; Kira, M.; Khitrova, G.; Gibbs, H. Semiconductor excitons in new light. *Nat. Mater.* **2006**, *5*, 523−531.
(40) Zhao, W.; Ghorannevis, Z.; Amara, K. K.; Pang, J. R.; Toh, M.; Zhang, X.; Kloc, C.; Tan, P. H.; Eda, G. Lattice dynamics in mono- and few-layer sheets of WS2 and WSe2. *Nanoscale* **2013**, *5*, 9677−9683.
(41) Du, L.; Liao, M.; Tang, J.; Zhang, Q.; Yu, H.; Yang, R.; Watanabe, K.; Taniguchi, T.; Shi, D.; Zhang, Q.; et al. Strongly enhanced exciton-phonon coupling in two-dimensional WSe2. *Phys. Rev. B: Condens. Matter Mater. Phys.* **2018**, *97*, 235145.
(42) Berkelbach, T. C.; Hybertsen, M. S.; Reichman, D. R. Theory of neutral and charged excitons in monolayer transition metal dichalcogenides. *Phys. Rev. B: Condens. Matter Mater. Phys.* **2013**, *88*, 045318.
(43) Kylänpää, I.; Komsa, H.-P. Binding energies of exciton complexes in transition metal dichalcogenide monolayers and effect of dielectric environment. *Phys. Rev. B: Condens. Matter Mater. Phys.* **2015**, *92*, 205418.
(44) Haastrup, S.; Strange, M.; Pandey, M.; Deilmann, T.; Schmidt, P. S.; Hinsche, N. F.; Gjerding, M. N.; Torelli, D.; Larsen, P. M.; Riis-Jensen, A. C.; et al. The Computational 2D Materials Database: high-throughput modeling and discovery of atomically thin crystals. *2D Mater.* **2018**, *5*, 042002.
(45) Liu, E.; van Baren, J.; Taniguchi, T.; Watanabe, K.; Chang, Y.-C.; Lui, C. H. Magnetophotoluminescence of exciton Rydberg states in monolayer WSe2. *Phys. Rev. B: Condens. Matter Mater. Phys.* **2019**, *99*, 205420.
(46) Raja, A.; Waldecker, L.; Zipfel, J.; Cho, Y.; Brem, S.; Ziegler, J. D.; Kulig, M.; Taniguchi, T.; Watanabe, K.; Malic, E.; et al. Dielectric disorder in two-dimensional materials. *Nat. Nanotechnol.* **2019**, *14*, 832−837.
(47) Brem, S.; Zipfel, J.; Selig, M.; Raja, A.; Waldecker, L.; Ziegler, J. D.; Taniguchi, T.; Watanabe, K.; Chernikov, A.; Malic, E. Intrinsic lifetime of higher excitonic states in tungsten diselenide monolayers. *Nanoscale* **2019**, *11*, 12381.
(48) Khatibi, Z.; Feierabend, M.; Selig, M.; Brem, S.; Linderälv, C.; Erhart, P.; Malic, E. Impact of strain on the excitonic linewidth in transition metal dichalcogenides. *2D Mater.* **2019**, *6*, 015015.
(49) Toyozawa, Y. Theory of line-shapes of the exciton absorption bands. *Prog. Theor. Phys.* **1958**, *20*, 53−81.
(50) Ivanov, A.; Haug, H. Self-consistent theory of the biexciton optical nonlinearity. *Phys. Rev. B: Condens. Matter Mater. Phys.* **1993**, *48*, 1490.
(51) Katsch, F.; Selig, M.; Carmele, A.; Knorr, A. Theory of Exciton−Exciton Interactions in Monolayer Transition Metal Dichalcogenides. *Phys. Status Solidi B* **2018**, *255*, 1800185.
(52) Cohen-Tannoudji, C.; Dupont-Roc, J.; Grynberg, G. Atom-photon interactions: basic processes and applications. *Atom-Photon Interactions: Basic Processes and Applications*; Wiley-VCH: New York, 1992.
(53) Selig, M.; Berghäuser, G.; Richter, M.; Bratschitsch, R.; Knorr, A.; Malic, E. Dark and bright exciton formation, thermalization, and photoluminescence in monolayer transition metal dichalcogenides. *2D Mater.* **2018**, *5*, 035017.
(54) Brem, S.; Selig, M.; Berghaeuser, G.; Malic, E. Exciton Relaxation Cascade in two-dimensional Transition Metal Dichalcogenides. *Sci. Rep.* **2018**, *8*, 8238.


https://dx.doi.org/10.1021/acs.nanolett.0c00633
*Nano Lett.* 2020, 20, 2849−2856

(55) Kira, M.; Jahnke, F.; Hoyer, W.; Koch, S. W. Quantum theory of spontaneous emission and coherent effects in semiconductor microstructures. *Prog. Quantum Electron.* **1999**, *23*, 189−279.
(56) Kira, M.; Koch, S. Many-body correlations and excitonic effects in semiconductor spectroscopy. *Prog. Quantum Electron.* **2006**, *30*, 155−296.
(57) Liu, E.; van Baren, J.; Lu, Z.; Altaiary, M. M.; Taniguchi, T.; Watanabe, K.; Smirnov, D.; Lui, C. H. Gate Tunable Dark Trions in Monolayer WSe2. *Phys. Rev. Lett.* **2019**, *123*, 027401.
(58) Christiansen, D.; Selig, M.; Berghäuser, G.; Schmidt, R.; Niehues, I.; Schneider, R.; Arora, A.; de Vasconcellos, S. M.; Bratschitsch, R.; Malic, E.; et al. Phonon sidebands in monolayer transition metal dichalcogenides. *Phys. Rev. Lett.* **2017**, *119*, 187402.
(59) Van Tuan, D.; Jones, A. M.; Yang, M.; Xu, X.; Dery, H. Virtual trions in the photoluminescence of monolayer transition-metal dichalcogenides. *Phys. Rev. Lett.* **2019**, *122*, 217401.
(60) Li, Z.; Wang, T.; Jin, C.; Lu, Z.; Lian, Z.; Meng, Y.; Blei, M.; Gao, S.; Taniguchi, T.; Watanabe, K.; et al. Emerging photoluminescence from the dark-exciton phonon replica in monolayer WSe2. *Nat. Commun.* **2019**, *10*, 2469.
(61) Liu, E.; van Baren, J.; Taniguchi, T.; Watanabe, K.; Chang, Y.-C.; Lui, C. H. Valley-selective chiral phonon replicas of dark excitons and trions in monolayer WS e 2. *Physical Review Research* **2019**, *1*, 032007.


https://dx.doi.org/10.1021/acs.nanolett.0c00633
*Nano Lett.* 2020, 20, 2849−2856